Biophysical Journal Volume 101 October 2011 1871–1879

Reversing Nerve Cell Pathology by Optimizing Modulatory Action on Target Ion Channels

Jenny Tigerholm[†‡] and Erik Fransén[†‡*]
[†]Department of Computational Biology, School of Computer Science and Communication and [‡]Stockholm Brain Institute, Royal Institute of Technology, Stockholm, Sweden

ABSTRACT In diseases of the brain, the distribution and properties of ion channels display deviations from healthy control subjects. We studied three cases of ion channel alteration related to epileptogenesis. The first case of ion channel alteration represents an enhanced sodium current, the second case addresses the downregulation of the transient potassium current K_A, and the third case relates to kinetic properties of K_A in a patient with temporal lobe epilepsy. Using computational modeling and optimization, we aimed at reversing the pathological characteristics and restoring normal neural function by altering ion channel properties. We identified two key aspects of neural dysfunction in epileptogenesis: an enhanced response to synaptic input in general and to highly synchronized synaptic input in particular. In previous studies, we showed that the potassium channel K_A played a major role in neural responses to highly synchronized input. It was therefore selected as the target upon which modulators would act. In biophysical simulations, five experimentally characterized endogenous modulations on the K_A channel were included. Relative concentrations of these modulators were controlled by a numerical optimizer that compared model output to predefined neural output, which represented a normal physiological response. Several solutions that restored the neuron function were found. In particular, distinct subtype compositions of the auxiliary proteins Kv channel-interacting proteins 1 and dipeptidyl aminopeptidase-like protein 6 were able to restore changes imposed by the enhanced sodium conductance or suppressed K_A conductance. Moreover, particular combinations of protein kinese C, calmodulin-dependent protein kinase II, and arachidonic acid were also able to restore these changes as well as the channel pathology found in a patient with temporal lobe epilepsy. The solutions were further analyzed for sensitivity and robustness. We suggest that the optimization procedure can be used not only for neurons, but also for other organs with excitable cells, such as the heart and pancreas where channelopathies are found.

INTRODUCTION

Epilepsy is a severe neurological disorder with a prevalence rate of 5–10 per 1000 individuals (1,2). There are many different forms of epilepsy, all characterized by spontaneous recurrent seizures. A seizure has a rich repertoire of events and one pronounced feature is highly synchronized neural activity (3). Synchronous input is very powerful in activating neurons (4) and therefore an enhanced neural response can therefore be part of the pathology. The underlying mechanisms generating the pathology are numerous. Sodium channels have been the major focus of epilepsy research involving ion channels (5). Both gene mutation studies and animal models have shown sodium current involvement in epileptogenesis (5,6). Other channels, such as the A-type potassium channel (K_A), have also been linked to epilepsy (7–10). In animal models, the K_A current and gene expression is downregulated (8,9). Furthermore, in a human genetic study a mutation in the K_A gene was linked to temporal lobe epilepsy (TLE) (7). When the mutated gene was expressed in human embryonic kidney cells, the K_A current was strongly reduced. Moreover, in a study on human epileptic tissue from a patient with TLE (10), it was shown that the K_A current had altered dynamics compared to the native current.

In epileptogenesis, a multitude of activity changes have been discussed, one of which is enhanced synchronicity at or before the onset of a seizure. Synchronous activity can generate compound excitatory postsynaptic potentials (EPSPs) with a fast rise time and high amplitude. Such input has been shown in vivo and in vitro to be particularly efficient in activating the neuron (11). Epileptic seizures are also characterized by excess spiking. Therefore, we have chosen to study neural excitability from the point of view of the generation of action potentials in response to synaptic input produced by network activity. To address excitability at the single neuron level, we focused on controlling the cellular spiking responses to different levels of synchronized input. In previous work (12), we studied the spiking of a neuron in response to the input of different degrees of synchronicity. We identified a particular potassium channel, K_A that was able to selectively reduce the neuronal responses to the most synchronized input. In the study presented here, we defined two goals: to reduce responses to highly synchronized input, representing activity during epileptogenesis, and to obtain a normal response to input of lower synchronicity levels corresponding to normal levels

Submitted April 15, 2011, and accepted for publication August 24, 2011.

*Correspondence: erikf@csc.kth.se

Jenny Tigerholm's and Erik Fransén's present address is Department of Computational Biology, School of Computer Science and Communication, Royal Institute of Technology, AlbaNova University Centre, Stockholm, Sweden.

Editor: Randall L. Rasmusson.

0006-3495/11/10/1871/9 $2.00

doi: 10.1016/j.bpj.2011.08.055

of excitability. These functional criteria were used as constraints for a numerical optimizer cost function. The pattern search method was chosen because it is a robust direct search method (13–15). We further analyzed the solutions we found in terms of parameter sensitivity and robustness.

In this study, we identified three cases of ion channel alterations associated with epileptogenesis. The first case showed enhanced sodium currents (16) and was represented in the model by increasing the transient sodium conductance. The second case of epilepsy addressed a downregulation of the K_A current (7) represented by reducing the K_A conductance. The third case is related to properties of K_A in a patient with temporal lobe epilepsy and was implemented using the measured biophysical properties. In a previous study, we showed that K_A may be beneficial in reducing epileptogenic activity (12). In this study, we focused on improving the functional behavior of the neuron and aimed at reversing the pathological change in neural response characteristics. We studied the modulation of K_A by intracellular messengers. There are many modulatory substances that modulate the K_A channel, such as auxiliary proteins, kinases, and polyunsaturated fatty acids (17–21). The main focus of this study was on subtypes of the two auxiliary proteins Kv channel-interacting proteins 1 (KChIP1) and dipeptidyl aminopeptidase-like protein 6 (DPP6) because of their selectivity to K_A. However, the study also included the modulatory substances protein kinase C (PKC), calmodulin-dependent protein kinase II (CaMKII), and arachidonic acid (AA). By using experimentally derived modulations of ion channel properties in the simulations, the solutions from the optimizer were the relative concentrations of the modulatory substances. These can be experimentally tested. If the compounds or their binding sites on K_A have suitable properties, they may be of interest for a pharmacological intervention.

MATERIALS AND METHODS

Cell model

All simulations were performed using the simulator NEURON (22). As a model of the physiological control condition, we used the CA1 pyramidal neuron model by Poolos et al. (23). The ion channels were described by Hodgkin-Huxley dynamics (see Supporting Material for the ionic equations). The model with no changes is referred to as the control model and models with changes are referred to as pathological models in the study.

During the simulation, 15 cycles of input were delivered for 1500 ms; each cycle consisted of one input each at 60 synapses activated at a particular degree of synchronicity. Fig. 1 *A* shows three examples of input synchrony, ranging from fully synchronized (all synapses activated at the same time) to relatively asynchronous input. Synchronicity is measured as the temporal standard deviation of the synaptic input and is generated from a normal distribution. As expected, the general trend was that more synchronized activity lead to the production of more spikes. However, note the reduced spike activity for synchronicity levels 0 and 1 ms (see Fig. 1 *C*), which corresponds to highly synchronized synaptic input. In our previous study, we showed that this low response is due to selective activation of K_A.

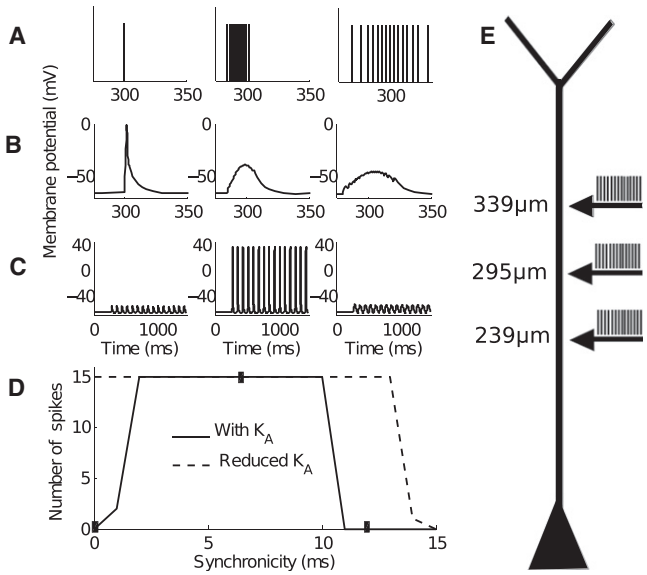

FIGURE 1 Neuron spiking response to different synchronicity levels. The three columns represent simulations with the following synchronicity levels; full (0 ms; *left*), medium (6 ms; *middle*), and low (12 ms; *right*) synchronicity of the inputs. Input was placed at three locations with the distance from the soma: 239, 295, and 339 μm. At each input location 20 synapses were placed. Arrival time for the temporal midpoint of the input is 300 ms. The same input was used for all figures if not stated otherwise. (*A*) Temporal distribution of the input. (*B*) Membrane potential at the input site for one input cycle. (*C*) The membrane potential in the soma for the full 1500 ms simulation. (*D*) Number of spikes produced for different levels of synchronized input, from fully synchronized (0 ms) to desynchronized (15 ms). We show the spike activity when K_A is present in the model (*blue*) and when the conductance of K_A is reduced with 40% (*black dotted line*). Note the strong reduction of spike activity in the 0–1 ms interval when K_A is present. Closed boxes correspond to synchronicity levels and spike counts shown in *C*. (*E*) The spatial distribution of the input. Each arrow corresponds to 20 synaptic contacts with the temporal distribution shown in *A*.

Models of epilepsy

A range of ion channels have been linked to epileptogenesis, particularly sodium and potassium channels. The involvement of the K_A channel in epileptogenesis has been studied in both animal models and in human tissue (7–9). Some of these studies show a downregulation of the gene expression or the current of K_A (24). The model describing this case was labeled reduced K_A model and was implemented as a reduction of the conductance of K_A by 50%.

The sodium channel has been strongly implicated in epileptogenesis, particularly since several gene mutations have been linked to epilepsy (6). A study on kindling epileptogenesis recorded a 22% increase in peak sodium current (16) and a 3 mV depolarizing shift of the steady-state inactivation curve. This model is referred to as the increased sodium model.

In human tissue from a patient with temporal lobe epilepsy (10), alterations in the dynamics of K_A have been described. The steady-state parameters from the study were implemented in a model labeled TLE model. The activation time constant was similar to data of native K_A and we therefore used the value of the control model. For more details of the models of the pathological models see Supporting Material.

The activity of the pathological cell models was measured for different levels of synchronized input, shown in Fig. 2. The pathological models had enhanced responses to highly synchronized input (synchronicity = 0–1 ms) and general excitability (synchronicity = 11–19 ms) was also increased for the models.

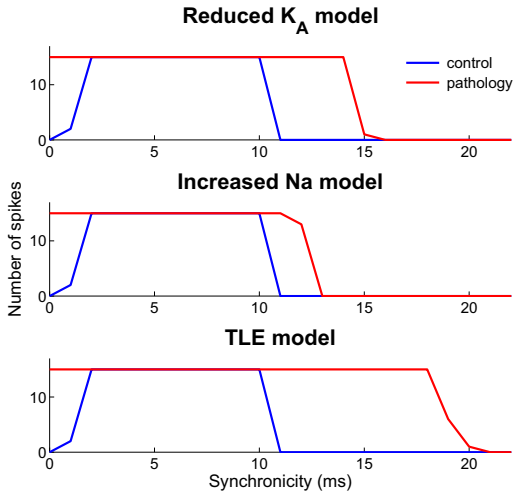

FIGURE 2 Increased excitability induced by pathological channel changes. The number of spikes produced for different levels of synchronicity is shown. Spiking in the control case is shown in blue and pathological cases are shown in red. The top trace shows the spike activity produced by the reduced K_A model, the middle shows the increased Na model, and the bottom trace the TLE model. Note the increased activity for all three pathological models to highly synchronized input (<2 ms) and to lower levels of synchronized input (>10 ms).

Models of modulatory substances

A short description of the implementation of the modulatory substance follows.

KChIP1

An upregulation of KChIP1 was modeled as an increase of the conductance of K_A and decrease of the inactivation time constant. If KChIP1 was downregulated the conductance was reduced and the inactivation time constant increased (see Supporting Material for the equation).

DPP6

DPP6 alters the $V_{1/2}$ of both the activation and inactivation steady-state functions as well as the inactivation time constant (18). This was implemented as a shift of the steady-state activation curve from a hyperpolarizing shift of 13.5 mV (highest relative concentration of DPP6) to a depolarizing shift of 13 mV (lowest relative concentration of DPP6). For the steady-state inactivation curve a shift from a hyperpolarizing shift of 7.5 mV to a depolarizing shift of 7.5 mV was used (corresponding to high and low relative concentration of DPP6). See Supporting Material for the description of the modulation of the inactivation time constant.

PKC

PKC activators downregulate the K_A current by shifting the steady-state activation curve (19). In the model, we implemented PKC modulation of K_A as a shift of the steady-state curve from a depolarizing shift of 15 mV to a hyperpolarizing shift of 15 mV (corresponding to high and low relative concentration of PKC).

AA

The polyunsaturated fatty acid AA shifts the steady-state inactivation curve 12 mV to more negative potentials (25). In the model, we implemented the modulation of AA as a shift of the steady-state inactivation curve from a hyperpolarizing shift of 12 mV to a depolarizing shift of 12 mV (corresponding to high and low relative concentration of AA).

CaMKII

Ca^{2+}/calmodulin-dependent protein kinase II (CaMKII) upregulates the channel expression of K_A without affecting the biophysical properties of K_A (20). CaMKII modulation of K_A was implemented as an up to twofold increase of the conductance of K_A. A decreasing level of CaMKII was implemented as a reduction of the conductance of K_A by a factor of up to two.

Functionally correcting the models of epilepsy by KChIP1 and DPP6

To reverse pathological changes, a numerical optimizer was used to search for improved models. We chose the pattern search method by Hook and Jeeves (15). It is a direct search algorithm, has a fast convergence, and handles a discontinuous cost function (13,14).

We defined the cost function so that the main goal of the optimizer was to functionally correct the pathological models. In this case, functionally corrected means a changed pathological model where a spiking output resembled the output of the control model (see Fig. 3 for a description of the optimization method). Basing a cost function on the number of generated spikes gives a discrete output that is produced by a threshold type of process. The use of a cost function described by small integers gives rise to slow optimizer convergence. We therefore used the membrane potential, which is a good predictor of spike activity, because spikes are produced by a process that is dependent on membrane potential. For a description of the cost function see Supporting Material. The optimizer found only one minimum when the relative proportions of subtypes of KChIPs or DPPs were the free variable. Fig. 3, *B–E*, shows the steps the optimizer chose to functionally correct the increased Na model.

RESULTS

For the reduced K_A model and increased sodium model, an increased concentration of KChIP1 could functionally correct spike activity (Fig. 4 and Table 1). Both these functionally corrected models could reduce highly synchronized input and normalize general excitability. Furthermore, by increasing the relative concentration of DPP6, a similar result could be attained (Fig. 4 and Table 1). In the increased sodium model, we noted that DPP6 reduced general excitability to levels below that of the control model. However, the TLE model could not be functionally corrected by changing either the relative concentration of KChIP1 or DPP6. This was due to limitations of the range of modulation by DPP6 and KChIP1. If instead a pure shift of the steady-state curves of K_A was used as a hypothetical modulator, the optimizer could find a solution (data not shown). This showed that the failure of the KChIP1 and DPP6 cases was not due to a shortcoming of the optimization process.

Fig. 5 shows the membrane potential during a simulation of the control model, the increased Na model, and its functionally corrected model by DPP6. In the pathological model, the cell was hyperexcitable for high synchronicity levels. In the functionally corrected model, the spike activity was very similar to the control case. Spike activity was reduced for the high synchronicity (<2 ms) and low synchronicity levels (>10 ms). The desynchronized input (2–5 ms) generated a high spike activity, as intended. However, the 6–10 ms interval generated spikes in the control model but not in the functionally corrected model.

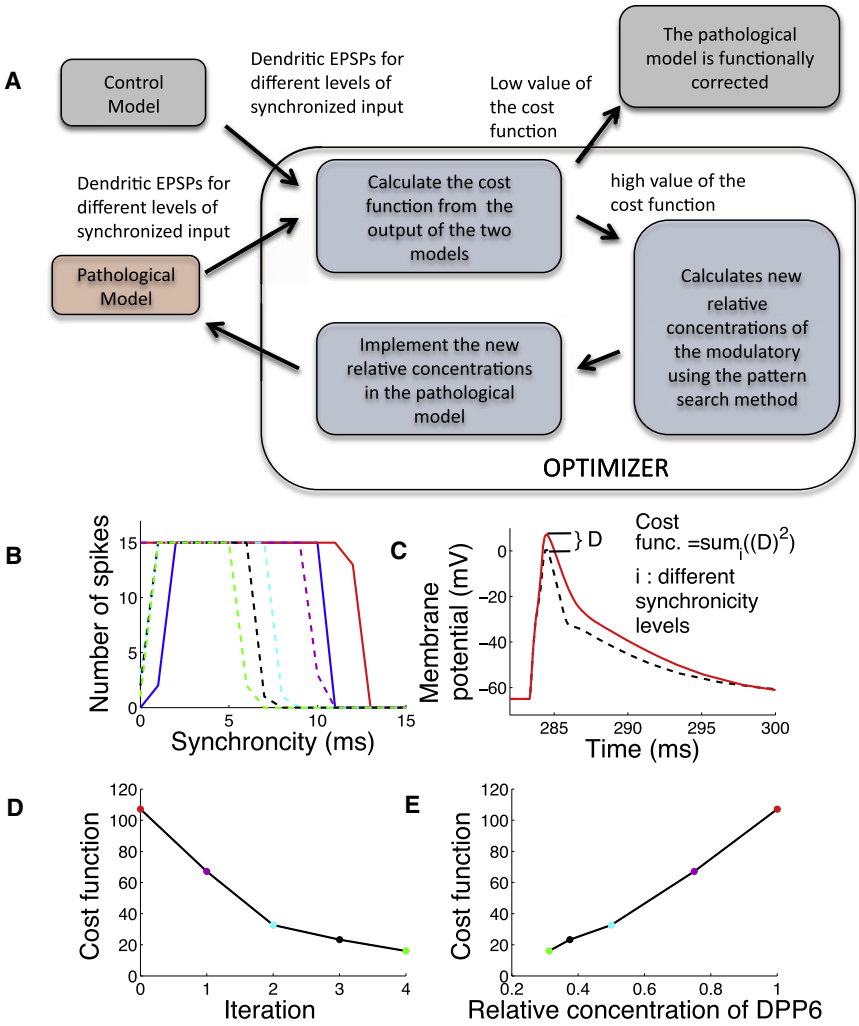

FIGURE 3 Optimization method. (*A*) The method we used to find functionally corrected models, starting with pathological models. The compound EPSP from the pathological model was compared to the control model to generate the cost value. If the cost value was high, new relative concentrations of the modulatory substances were calculated by the pattern search method. The new concentrations were then implemented in the model, a new simulation was run, and a new set of EPSPs were generated. A new cost value was computed and when this fell below the stop criteria the model was labeled functionally corrected. (*B*) The spiking response for different synchronicity levels during the optimization procedure. The starting point of the optimization is the pathological model (*red*) and the goal is the control model (*blue*). For illustration, spike activity for each iteration during the optimization is also shown (*dashed lines*). Final solution found is indicated in green. Each color in *B*, *D*, and *E* corresponds to the same iteration cycle. (*C–E*) Illustrates the optimization cycle. (*C*) Dendrite membrane potential produced in a control case (*blue*) and a pathological case (*red*). The difference in peak EPSP amplitude at the input site for the first and second input cycles were used to calculate the cost function value. (*D*) The cost function value for each iteration during the optimization. (*E*) The relative concentration of DPP6 for each iteration of the optimization.

To study the ability of K_A to reduce synchronized input we measured the membrane potential at different locations along the dendrite when a depolarization was propagating to the soma (see Fig. 5 *D*). In Fig. 5 *D* we show the membrane potential for the functionally corrected model (DPP6) and the increased sodium model. At the synaptic input site (240 μm from the soma) the two models have a similar depolarization for high levels of synchronized input, however during the propagation to the soma the two models diverge. The pathological model generates a spike but the functionally corrected model does not. Fig. 5 *D* shows that the ability of K_A to reduce synchronized input is a filtering process along the dendrite.

Sensitivity analysis on the functionally corrected model modulated by DPP6

A variance-based sensitivity analysis (26) was used to investigate how the different modulatory effects of DPP6 influenced spike activity. Fig. 6 *A* shows the first-order sensitivity index for the functionally corrected increased Na model. The sensitivity index measures the influence of a specific parameter on one feature of the model, in this case the spike activity (see Supporting Material for further information). The parameters used for this analysis were the different effects of DPP6 on K_A; shifting the steady-state activation curve, shifting the inactivation steady-state curve, and a change in the inactivation time constant. We note that the largest impact comes from the steady-state activation curve shift (Fig. 6 *A*). Fig. 6 *A* shows the sensitivity index when the intervals of change were set to $\pm$ 10%. The spike activity for desynchronized input (1–4 ms) was not affected by the changes. For high synchronicity levels (0–1 ms) the first-order sensitivity index is large. However, if we plot the variance (i.e., the without normalizing by the mean), we see that the actual number of spikes is quite small (see Fig. 6 *B*). Together, this indicates that the solution found is robust in reducing highly synchronized input. The variance-based sensitivity analysis indicated that the DPP6 modulation on K_A might be simplified. In Fig. 6 *C*, the three different modulations of K_A were removed one at a time from the model and we tested whether the model was still functionally corrected. Only the modulation of the steady-state inactivation time constant

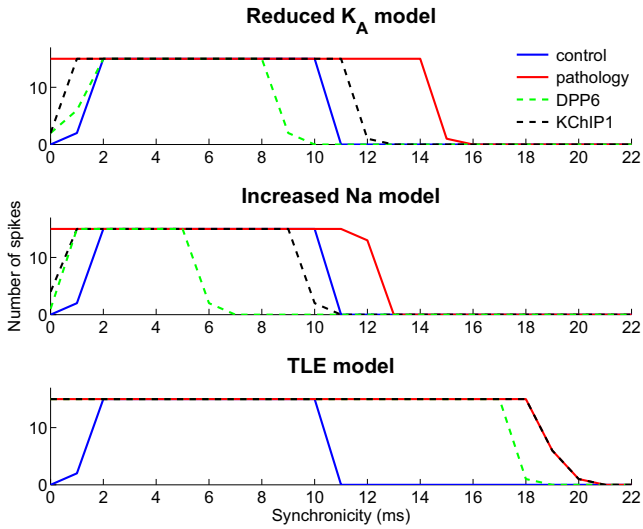

FIGURE 4 DPP6 and KChIP1 can functionally correct two of the pathological models. The figure shows spike activity during control conditions (*blue*) and spike activity for the pathological models (*red*). The top trace shows the spike activity produced by the reduced K_A model, the middle increased Na model, and the bottom the TLE model. We show the functionally corrected pathological models (*dotted lines*) when KChIP1 was used as a free variable (*black*) and when DPP6 was used as the free variable (*green*).

could be removed without major effects on the degree to which the model is functionally corrected. The three modulations of DPP6 affect the excitability of the cell differently. The steady-state activation and inactivation time constant modulation both reduce the excitability of the model. The steady-state inactivation modulation, on the contrary increases the excitability. Simplifying the model of how modulation of DPP6 changes the properties of K_A is therefore not trivial.

Functionally correcting the models of epilepsy by PKC, AA, and CaMKII

The properties of ion channels are subject to dynamic modulatory balance (27). K_A changes depending on its kinetic properties following, e.g., phosphorylation. We therefore extended our analysis to include modulatory alterations of PKC (19) and CaMKII (20) as well as the lipid messenger AA (25). First, the effects of the modulatory substances were studied one by one and second, because PKC, AA, and CaMKII do not have a strong mutual interaction regarding their effects on K_A, their combined affect was studied.

When PKC, CaMKII, and AA were studied in isolation both the reduced K_A model and increased Na model could be functionally corrected but not the TLE model (see Fig. 7). However, three free parameters PKC, AA, and CaMKII together, could functionally correct all three pathological models (see Fig. 7). For the reduced K_A and increased Na model, multiple minima could be found. The solutions are presented in the Table 1.

Sensitivity and robustness analysis on the functionally corrected model by PKC, AA, and CaMKII

Results from the increased Na model were further analyzed. The three solutions with the lowest cost function score are

TABLE 1 Parameter values for solutions found by the optimizer

	Relative concentration of the substance	Shift of the steady-state activation curve (mV)	Shift of the steady-state inactivation curve (mV)	Conductance change (%)
KChIP1 red. K_A	2.00	–	–	1.71
inc. Na	1.63			1.45
DPP6 red. K_A	1.80	−9.28	−5.16	–
inc. Na	1.69	−10.8	−6.00	
PKC red. K_A	0.21	−11.9	-	–
inc. Na	0.34	−9.90		
CaMKII red. K_A	1.80	–	-	1.80
inc. Na	1.72			1.72
AA red. K_A	0.00	–	12.0	–
inc. Na	0.00		12.0	
Solution A				
PKC, CaMKII, AA red. K_A	0.52 1.66 1.53	−7.18	−6.36	1.66
inc. Na	1.13 1.67 0.44	1.94	6.72	1.67
TLE	0.00 2.00 0.00	−15.0	12.0	2.00
Solution B				
PKC, CaMKII, AA red. K_A	0.73 1.73 1.30	−4.13	−3.60	1.73
inc. Na	0.79 1.27 0.62	−3.08	4.44	1.27
Solution C				
PKC, CaMKII, AA red. K_A	0.40 1.77 1.73	−9.08	−8.70	1.77
inc. Na	0.72 1.47 1.21	−4.17	−2.50	1.47

Solutions found by the optimizer for the pathologies. In the table the alteration of the steady-state curves and conductance for the different solutions are shown. Negative shifts correspond to a hyperpolarizing shift of a steady-state curve and positive shift to a depolarizing shift of the steady-state curve. The inactivation time constant alterations are described in the Supporting Material.

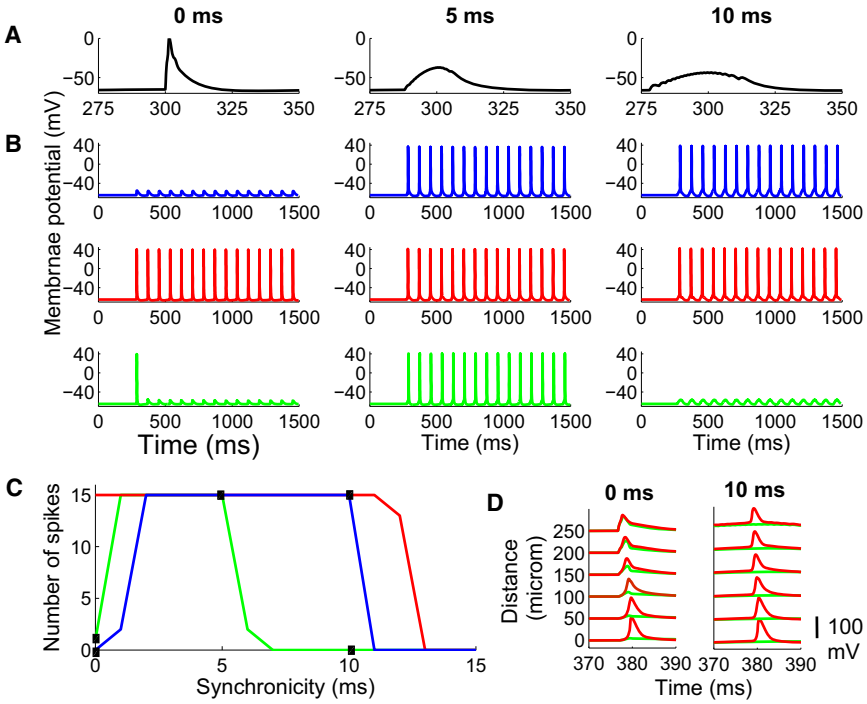

FIGURE 5 Membrane potentials for the functionally corrected increased Na model by DPP6. The three columns in *A* and *B* represent simulations with synchronicity levels of 0 ms (*left*), 5 ms (*middle*), and 10 ms (*right*). The first input cycle was set to have a midpoint at 300 ms. (*A*) The membrane potential at the input site in the control model. (*B*) The membrane potential in the soma in the control model (*blue*), pathological model (*red*), and functionally corrected model (*green*). (*C*) The spike activity for different levels of synchronized input. The control model (*blue*), the increased Na model (*red*), and the functionally corrected model (*green*) are shown. Boxes indicate synchronicity levels used in the three columns in the traces above. (*D*) The membrane potential from the increased Na model (*red*) and functionally corrected model corrected by DPP6 (*green*) are shown. The left column shows the simulation with 0 ms and the right column with 10 ms synchronicity. The different rows (*top to bottom*) show the membrane potential at decreasing distances from the soma. Note for the left column how the EPSP amplitude is decreased when it propagates to the soma.

shown in Fig. 8. Because there were multiple functionally corrected model solutions for each pathological model, this gave rise to the question of which solution was the preferred one. Not only was it important for the model to be functionally corrected, but we also wanted an adequate level of parameter sensitivity (not too sensitive for parameters relevant to the problem, but at the same time not totally indifferent). Furthermore, the robustness of the solution is also highly important. If small alterations to the model lead to an output that is characteristic of a pathological model, the model will in the following be termed not robust. Robustness can thus be viewed as the parameter interval within which the model produces output that is classified as functionally corrected.

As a first step into examining the quality of the solutions, we measured the spike variance when the input variables (PKC, AA, and CaMKII) were varied within $\pm 19\%$ of the allowed parameter interval. The three models had similar spike activity dependencies (see Fig. 8). Notice that the variance for synchronicity levels between 2 and 4 ms is low. This meant that the solutions were not sensitive in the region where a maximum firing of the neuron was expected.

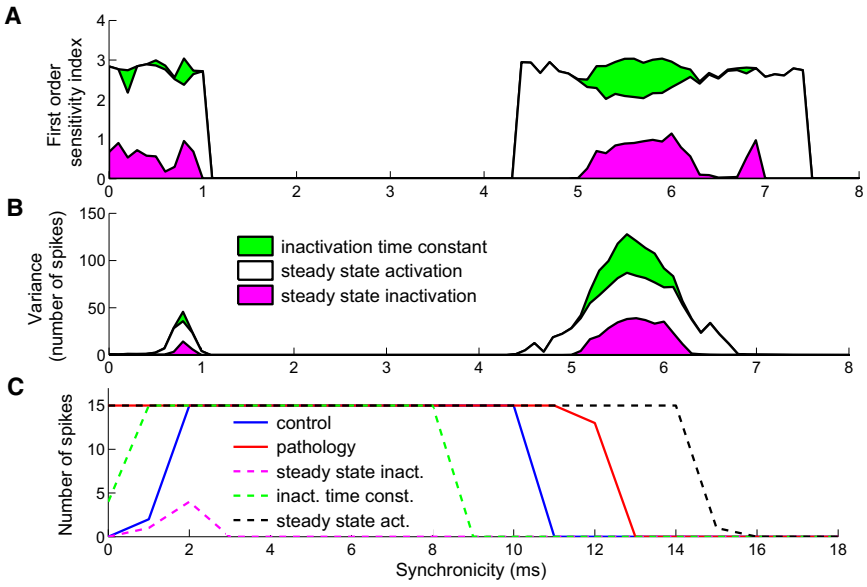

FIGURE 6 Sensitivity analysis. (*A*) Variance-based sensitivity analysis of the corrected increased Na model corrected by DPP6. Interval of variation was $\pm 10\%$ of the parameter interval. (*B*) Variance of spike activity (nonnormalized sensitivity index) when the effects from DPP6 on the K_A channel were varied one at a time. (*C*) Spike activity is shown when one modulation property at a time (out of the three included) was omitted in the functionally corrected model of reduced Na pathology corrected by DPP6. Spike activity in the pathological model with increased Na (*red*), and the control model (*blue*) are shown. The dotted curves represent cases where one modulation was omitted, showing inactivation time constant (*green*), steady-state activation (*black*), and steady-state inactivation (*purple*).

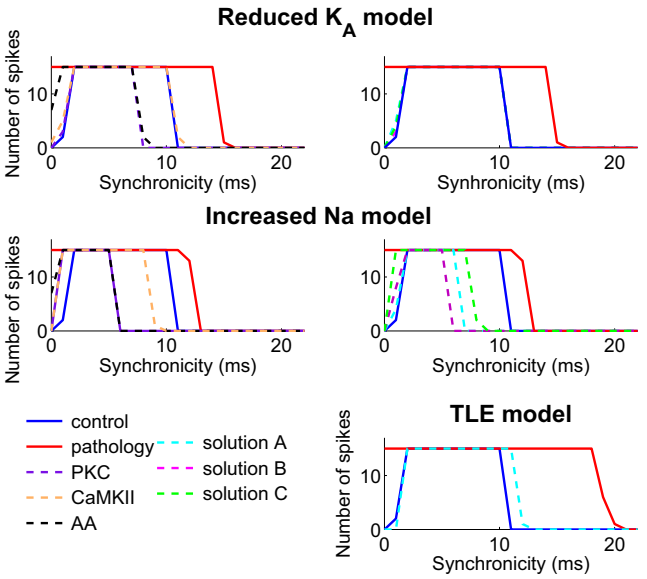

FIGURE 7 PKC, AA, and CaMKII can functionally correct all pathological models. The figure shows the spike activity for the functionally corrected models (*dotted lines*), pathological models (*red*), and the control model (*blue*). The top trace represents the reduced K_A model, middle the increased Na model, and bottom the TLE model. The left column shows solution when the PKC (*purple*), CaMKII (*orange*), and AA (*black*) effect is studied in isolation and the right the combinations of them. If there exist multiple solutions, the three best functionally corrected models (A in *light blue*, B in *pink*, and C in *green*) are shown.

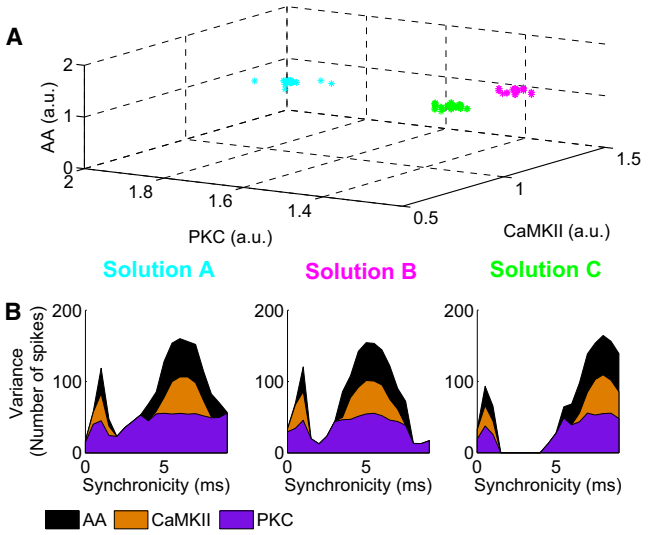

FIGURE 8 Sensitivity analysis. Results from the increased Na model, solution A *(blue)*, B *(pink)*, C *(green)*. (*A*) Data points visited by the optimizer with a cost function value below two are shown. Axes values are in arbitrary concentration units. (*B*) Variance of spike activity in the functionally corrected increased Na model when PKC (*purple*), CaMKII (*orange*), and AA (*black*) were changed by $\pm 19\%$ of the parameter interval. The left column represents solution A, the middle column solution B, and right column solution C.

However, in such important regions as the high synchronicity region of 0–2 ms and the low synchronicity region of 4–9 ms, they were sensitive and thus contributed to the model behavior. Fig. 8 *B* also shows that PKC is the most influenced modulatory substance on the spiking output compared.

Second, the solutions were examined in terms of their robustness. To measure the robustness of a solution, a parameter value of the solution was increased or decreased until the model was not classified as functionally corrected (see Supporting Material for more information). The sum of the two intervals (the increased and decreased) was defined as the width of the parameter (see Table 2). Solution B (*pink* in Fig. 7) had the lowest cost function value but smaller width than solution A and C (*light blue* and *green* in Fig. 7). When the minima were examined closer, the minima of solution A were not symmetrical. For instance, PKC could be increased by a factor of 20% but could merely be decreased $<5\%$. All the parameters, which in this way could only be decreased or increased by $<10\%$, are highlighted in bold in Table 2. The robustness score was decreased by one upon each such occurrence. Solution C had the highest robustness score and the two other solutions B and A had considerably lower robustness scores.

To extend the robustness analysis of the solutions, the relative concentration found by the optimizer were implemented in the model by Poirazi et al. (28). We choose the Poirazi model because it is one of the most well-studied models of dendritic integration. A similar result could be obtained in the Poirazi model, 7 of 10 solutions were functionally corrected. See Supporting Material for more information.

DISCUSSION

We studied how a combination of parameter search optimization and simulation of a biophysical neuron model could be used to reverse pathological cellular signatures and thereby restore normal neuronal function. We applied the procedure to three cases of ion channel disturbances linked to epileptogenesis. Modulations of the potassium channel K_A, as reported for the auxiliary proteins KChIPs and DPPs, could restore two of the cases; a decreased conductance of K_A and an increased conductance of a sodium channel. Conversely, changed levels of KChIPs and DPPs were unable to functionally restore ion channel alteration of K_A measured in a patient suffering from temporal lobe epilepsy. However, using modulation of K_A by the three modulatory substances PKC, CaMKII, and AA, we could functionally correct the alteration due to the pathology in all three cases.

We chose the optimization method developed by Hook and Jeeves (15). It is a direct search algorithm and thereby does not rely on computing derivatives. It has a fast convergence and can handle a discontinuous cost function (13,14). We found the pattern search method to be stable and fast enough to be useful for the optimization problem we have

TABLE 2 Characterization of three best solutions for multidimensional search

Solution	Cost function value	Width*	Relative concentration of PKC (%)	Relative concentration of CaMKII (%)	Relative concentration of AA (%)	Robustness score†
A (blue)	1.0232	1.56	−**5**–+20	−30–+20	−15–+65	−1
B (pink)	0.0003	1.00	−**0**–+20	−25–+**0**	−**0**–+55	−3
C (green)	0.0069	2.05	−25–+20	−25–+65	−35–35	0

Characterization of three best solutions. For the three best solutions, A–C, the cost function value at the minima, the width of the minima, the endpoints of the width, and the robustness score are shown. If a small change (<10%) can lead to epileptic behavior, the endpoint is indicated in bold and the robustness is decreased by one. Solutions are labeled by color as in Figs. 7 and 8.

*Sum of the absolute value of columns 4, 5, and 6.

†Number of nonrobust interval endpoints in the columns 4, 5, and 6.

focused on in this study. We have used a variance-based sensitivity analysis (26) to investigate the sensitivity and to estimate the influence of the different model parameters. The analysis showed that our target channel K_A exerts very little influence for semisynchronized input, in our study considered as normal brain activity. However, it played a significant role in both suppression of highly synchronized input and in controlling input of low synchronicity. This supports the selective role of K_A in suppressing synchronous neural activity as well as controlling general excitability.

Native K_A is coassembled with auxiliary proteins, KChIPs and DPPs (18). The subunit composition affects the kinetic properties of the channel in terms of shifts of the steady-state activation and inactivation curves as well as changes in time constants of activation and inactivation. These changes in characteristics form the basis of our study because they determine what dimensions the optimizer is allowed to affect. In our study changes due to DPP6s were implemented according to data from DPP6 expression data (18), which are consistent with DPP6 knockdown studies (29). Effects on steady-state curves and time constants have also been found for DPP10 (30) as well as for splice variants of DPP6 (31). In the former case, shifts of the type we used in our work would result from changes in the balance of DPP6 versus DPP10 and in the latter case between, e.g., changes in the balance between DPP6a and DPP6L. Although every case above would give a unique set of changes in properties, our study shows that the robustness of the solutions found indicate that solutions could be experimentally achieved in a number of experimental settings.

Several animal models of epilepsy have shown a reduction of the K_A current or gene/mRNA expression (8,24). Moreover, the KChIP1 gene expression is also downregulated by seizures (32). This rundown of KChIP1 also leads to a reduced K_A current that further increases the probability for new seizures, potentially generating a vicious circle. To address this problem, we implemented a model with a reduced K_A conductance. This pathological model was hyperexcitable both for high and low synchronicity levels. Our simulations showed that an increase of KChIP1 (relative concentration = 2) or of DPP6 (relative concentration = 1.80) could functionally correct the pathological model's response to different levels of synchronized input.

In a third model of pathology, we implemented the dynamics of K_A measured in a patient with temporal lobe epilepsy. The steady-state parameters for the pathological K_A were altered substantially with respect to the native parameters (33–35). The steady-state inactivation function was shifted 45 mV in the hyperpolarizing direction and the steady-state activation function 10 mV in the same direction. Due to the large alteration in the dynamics of K_A, neither KChIP1 nor DPP6 were able to functionally correct this case. The limitations stem from the limits of the modulation range in K_A kinetics, which these substances can exert on the K_A channel. Several splice variants of KChIP1 and DPP6 exist and if effects from several of these were included simultaneously in the model, the model might become functionally corrected. This was not tested in this study, as the interaction between these variants and how they summate is currently unknown. However, in the case where PKC, CaMKII, and AA modulations were combined, this pathology could be functionally corrected. PKC and CaMKII affect many essential cellular processes and are therefore not selective to K_A. Using these to directly reduce epileptic activity would produce several side effects. As an alternative, compounds selective to K_A that phosphorylate the same phosphorylation sites as PKC and CaMKII might be used. Furthermore, AA and other polyunsaturated fatty acids are already used for treatment of epilepsy (36). In several studies, children with epilepsy were put on a high fat, low-carbohydrate diet, leading to a reduced occurrence of seizures (36,37). The target of the anticonvulsant effect is still unknown. Our results support the possible beneficial role of action on K_A.

The results of this study indicate that changes in ion channel characteristics induced by modulatory substances may be beneficial in reducing epileptogenic activity. The method we developed to functionally correct a pathological neuron can be used for other brain diseases where alterations of ion channels are involved. It may also be used in other organs with excitable cells, such as the heart or pancreas. For instance, atrial fibrillation is one of the most common sustained cardiac arrhythmias with an underlying pathology of cell hyperexcitability due to, among other things, alterations of ion channels (38).

SUPPORTING MATERIAL

Additional details, seven figures, and references are available at http://www.biophysj.org/biophysj/supplemental/S0006-3495(11)01068-X.

We thank Maya Brandi and Yishao Zhou for valuable discussions on optimization methods, and Sara Soltani and Cathleen Heil for their summer internship work. We also thank Fredrik Elinder, Henry Jerng, and Paul Pfaffinger for valuable discussions.

REFERENCES

1. Sander, J. W., and S. D. Shorvon. 1987. Incidence and prevalence studies in epilepsy and their methodological problems: a review. *J. Neurol. Neurosurg. Psychiatry.* 50:829–839.
2. Semah, F., M. C. Picot, …, M. Baulac. 1998. Is the underlying cause of epilepsy a major prognostic factor for recurrence? *Neurology.* 51:1256–1262.
3. McNamara, J. O. 1999. Emerging insights into the genesis of epilepsy. *Nature.* 399(6738, Suppl):A15–A22.
4. Azouz, R., and C. M. Gray. 1999. Cellular mechanisms contributing to response variability of cortical neurons in vivo. *J. Neurosci.* 19:2209–2223.
5. Köhling, R. 2002. Voltage-gated sodium channels in epilepsy. *Epilepsia.* 43:1278–1295.
6. Meisler, M. H., and J. A. Kearney. 2005. Sodium channel mutations in epilepsy and other neurological disorders. *J. Clin. Invest.* 115:2010–2017.
7. Singh, B., I. Ogiwara, …, K. Yamakawa. 2006. A Kv4.2 truncation mutation in a patient with temporal lobe epilepsy. *Neurobiol. Dis.* 24:245–253.
8. Bernard, C., A. Anderson, …, D. Johnston. 2004. Acquired dendritic channelopathy in temporal lobe epilepsy. *Science.* 305:532–535.
9. Castro, P. A., E. C. Cooper, …, S. C. Baraban. 2001. Hippocampal heterotopia lack functional Kv4.2 potassium channels in the methylazoxymethanol model of cortical malformations and epilepsy. *J. Neurosci.* 21:6626–6634.
10. Rüschenschmidt, C., R. Köhling, …, E. J. Speckmann. 2004. Characterization of a fast transient outward current in neocortical neurons from epilepsy patients. *J. Neurosci. Res.* 75:807–816.
11. Azouz, R., and C. M. Gray. 2003. Adaptive coincidence detection and dynamic gain control in visual cortical neurons in vivo. *Neuron.* 37:513–523.
12. Fransén, E., and J. Tigerholm. 2010. Role of A-type potassium currents in excitability, network synchronicity, and epilepsy. *Hippocampus.* 20:877–887.
13. Kolda, T. G., R. M. Lewis, and V. Torczon. 2003. Optimization by direct search: new perspectives on some classical and modern methods. *Soc. Ind. Appl. Math.* 45:385–482.
14. Torczon, V. 1997. On the convergence of pattern search algorithms. *SIAM J. Optim.* 7:1–25.
15. Hook, R., and T. A. Jeeves. 1961. Direct search solution of numerical and statistical problems. *J. Assoc. Comp.* 8:212–229.
16. Vreugdenhil, M., G. C. Faas, and W. J. Wadman. 1998. Sodium currents in isolated rat CA1 neurons after kindling epileptogenesis. *Neuroscience.* 86:99–107.
17. An, W. F., M. R. Bowlby, …, K. J. Rhodes. 2000. Modulation of A-type potassium channels by a family of calcium sensors. *Nature.* 403:553–556.
18. Maffie, J., and B. Rudy. 2008. Weighing the evidence for a ternary protein complex mediating A-type K^+ currents in neurons. *J. Physiol.* 586:5609–5623.
19. Hoffman, D. A., and D. Johnston. 1998. Downregulation of transient K^+ channels in dendrites of hippocampal CA1 pyramidal neurons by activation of PKA and PKC. *J. Neurosci.* 18:3521–3528.
20. Varga, A. W., L. L. Yuan, …, J. D. Sweatt. 2004. Calcium-calmodulin-dependent kinase II modulates Kv4.2 channel expression and upregulates neuronal A-type potassium currents. *J. Neurosci.* 24:3643–3654.
21. Boland, L. M., and M. M. Drzewiecki. 2008. Polyunsaturated fatty acid modulation of voltage-gated ion channels. *Cell Biochem. Biophys.* 52:59–84.
22. Hines, M. L., and N. T. Carnevale. 1997. The NEURON simulation environment. *Neural Comput.* 9:1179–1209.
23. Poolos, N. P., M. Migliore, and D. Johnston. 2002. Pharmacological upregulation of h-channels reduces the excitability of pyramidal neuron dendrites. *Nat. Neurosci.* 5:767–774.
24. Francis, J., D. G. Jugloff, …, J. H. Eubanks. 1997. Kainic acid-induced generalized seizures alter the regional hippocampal expression of the rat Kv4.2 potassium channel gene. *Neurosci. Lett.* 232:91–94.
25. Angelova, P., and W. Müller. 2006. Oxidative modulation of the transient potassium current IA by intracellular arachidonic acid in rat CA1 pyramidal neurons. *Eur. J. Neurosci.* 23:2375–2384.
26. Saltelli, A., S. Tarantola, F. Campolongo, and M. Ratto. 2004. Sensitivity Analysis in Practice: A Guide to Assessing Scientific Models. John Wiley & Sons, Chichester.
27. Pedarzani, P., M. Krause, T. Haug, J. F. Storm, and W. Stühmer. 1998. Modulation of the Ca^{2+}-activated K^+ current sIAHP by a phosphatase-kinase balance under basal conditions in rat CA1 pyramidal neurons. *J. Neurophysiol.* 79:3252–3256.
28. Poirazi, P., T. Brannon, and B. W. Mel. 2003. Arithmetic of subthreshold synaptic summation in a model CA1 pyramidal cell. *Neuron.* 37:977–987.
29. Kim, J., M. S. Nadal, …, D. A. Hoffman. 2008. Kv4 accessory protein DPPX (DPP6) is a critical regulator of membrane excitability in hippocampal CA1 pyramidal neurons. *J. Neurophysiol.* 100:1835–1847.
30. Jerng, H. H., K. Kunjilwar, and P. J. Pfaffinger. 2005. Multiprotein assembly of Kv4.2, KChIP3 and DPP10 produces ternary channel complexes with I_{SA}-like properties. *J. Physiol.* 568:767–788.
31. Nadal, M. S., Y. Amarillo, E. Vega-Saenz de Miera, and B. Rudy. 2006. Differential characterization of three alternative spliced isoforms of DPPX. *Brain Res.* 1094:1–12.
32. Su, T., W. D. Cong, …, W. P. Liao. 2008. Altered expression of voltage-gated potassium channel 4.2 and voltage-gated potassium channel 4-interacting protein, and changes in intracellular calcium levels following lithium-pilocarpine-induced status epilepticus. *Neuroscience.* 157:566–576.
33. Hoffman, D. A., J. C. Magee, C. M. Colbert, and D. Johnston. 1997. K^+ channel regulation of signal propagation in dendrites of hippocampal pyramidal neurons. *Nature.* 387:869–875.
34. Martina, M., J. H. Schultz, …, P. Jonas. 1998. Functional and molecular differences between voltage-gated K^+ channels of fast-spiking interneurons and pyramidal neurons of rat hippocampus. *J. Neurosci.* 18:8111–8125.
35. Bekkers, J. M. 2000. Properties of voltage-gated potassium currents in nucleated patches from large layer 5 cortical pyramidal neurons of the rat. *J. Physiol.* 525:593–609.
36. Xu, X. P., D. Erichsen, …, F. Elinder. 2008. Polyunsaturated fatty acids and cerebrospinal fluid from children on the ketogenic diet open a voltage-gated K channel: a putative mechanism of antiseizure action. *Epilepsy Res.* 80:57–66.
37. Freeman, J. M., E. P. Vining, …, L. M. Kelly. 1998. The efficacy of the ketogenic diet-1998: a prospective evaluation of intervention in 150 children. *Pediatrics.* 102:1358–1363.
38. Li, Q., H. Huang, …, M. H. Gollob. 2009. Gain-of-function mutation of Nav1.5 in atrial fibrillation enhances cellular excitability and lowers the threshold for action potential firing. *Biochem. Biophys. Res. Commun.* 380:132–137.